

# Heat and Metal Transfer in Gas Metal Arc Welding Using Argon and Helium

P.G. JÖNSSON, T.W. EAGAR, and J. SZEKELY

This article describes a theoretical investigation on the arc parameters and metal transfer in gas metal arc welding (GMAW) of mild steel using argon and helium shielding gases. Major differences in the predicted arc parameters were determined to be due to large differences in thermophysical properties. Various findings from the study include that an arc cannot be struck in a pure helium atmosphere without the assistance of metal vapor, that a strong electromagnetic cathode force affects the fluid flow and heat transfer in the helium arc, providing a possible explanation for the experimentally observed globular transfer mode and that the tapering of the electrode in an argon arc is caused by electron condensation on the side of the electrode.

## I. INTRODUCTION

THE shielding gas composition is a critical process variable that influences the operation of gas metal arc welding (GMAW).<sup>[1]</sup> In general, the shielding gas protects the electrode and the workpiece from contaminants in the atmosphere, acts as a medium in which a current can flow to sustain an arc, and affects the shape of the weld bead and the resulting mechanical properties of the weldment. This investigation focuses on the influence of argon and helium upon the arc parameters, tapering of the electrode, and metal transfer in GMAW of mild steel.

Though both argon and helium are inert gases, most of their other properties are markedly dissimilar. One of the important characteristics of a shielding gas is its ionization potential, which reflects the tendency of a gas to ionize. The first ionization potentials, representing the loss of one electron, for argon and helium are 15.755 and 24.580 V, respectively.<sup>[2]</sup> The lower ionization potential of argon indicates that it is ionized at a lower voltage than helium and therefore can strike an arc more easily. The lower ionization potential of argon also means a lower power (arc voltage  $\times$  current) in the arc, which results in a more shallow weld penetration, undercutting and a poor weld bead contour.<sup>[3]</sup> Helium's higher ionization potential requires a higher voltage to ionize the gas and to provide a current flow large enough to sustain the arc. The higher arc voltage of helium, resulting in high arc power density, produces a more contracted arc and a smaller cathode spot. The intense and contracted helium arc column also results in greater penetration than for the argon shielding gas. The cost of helium is higher than for argon, which is a commercial disadvantage. Helium, however, is still used in the industry for high conductivity materials due to its ability to produce welds at higher speeds.<sup>[4]</sup>

Originally, the intent of this investigation was to provide a comparison of the arc parameters of a pure helium and a pure argon shielded arc. However, the arc calculations using the properties for pure helium did not

converge. The electrical conductivity of pure helium was not high enough to sustain an arc at the lower temperatures that exist close to the anode and the cathode. Instead, a 90 pct helium-10 pct iron vapor gas mixture was used in the calculations. A more in-depth explanation is given in Section IV.

In Section II, the general characteristics of the GMAW process are discussed. Section III presents details of the theoretical calculation of the arc parameters. The thermophysical properties for argon and helium are then compared in Section IV. Thereafter, some results are presented in Section V of typical arc parameters: electric potential, electromagnetic body force, mass flow, and temperature. The following topics related to metal transfer are also discussed: tapering of the electrode and repelled globular transfer mode.

## II. BACKGROUND

Figure 1 shows the main components of the GMAW system, which consists of the consumable electrode (anode), the anode-fall region, the arc column, the cathode-fall region and the workpiece (cathode). This figure also includes the gas-shielding nozzle, through which the shielding gas is supplied to the arc.

When an arc is struck between the anode and the cathode, a current flows through the electric discharge created between the electrodes. The arc current spreads laterally from the anode spot and a jet is formed, which gives rise to a flow in the direction of the cathode (workpiece). The gas impinges on the workpiece and is spread in a direction parallel to the workpiece. Also, the current distribution at the anode gives rise to a high heat generation in the near anode area, which results in rapid melting of the consumable electrode. Droplets form at the melted electrode tip, detach from the electrode, and are transferred to the workpiece under the influence of arc forces. The melted droplets solidify at the workpiece and form part of the welded joint.

## III. THEORETICAL MODEL

A two-dimensional steady-state mathematical model has been developed to predict arc parameters such as

P.G. JÖNSSON, formerly Graduate Student, Massachusetts Institute of Technology, is Head of Secondary Metallurgy Group with MEFOS, Luleå, Sweden. T.W. EAGAR and J. SZEKELY, Professors, are with the Department of Materials Science and Engineering, Massachusetts Institute of Technology, Cambridge, MA 02139.

Manuscript submitted August 11, 1993.

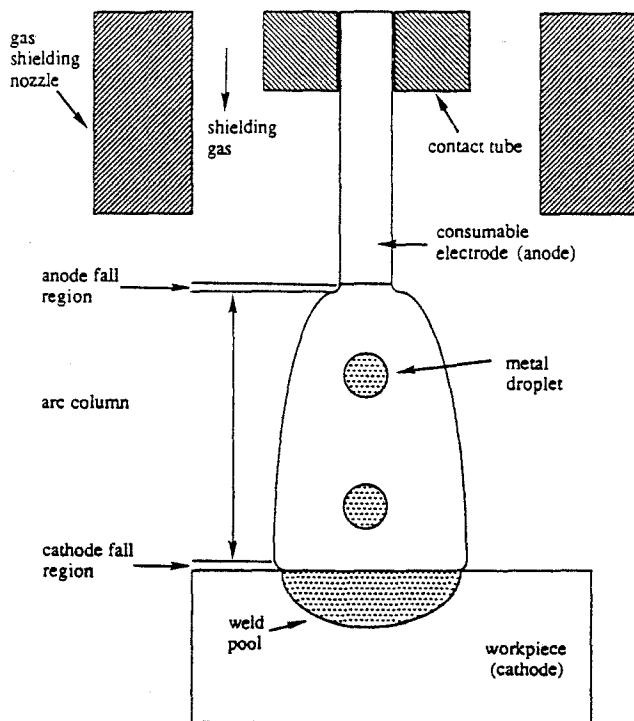


Fig. 1—The gas metal arc welding system.

electric potential, temperature, and velocity. In an earlier study, the model was applied to GMAW of aluminum in an argon atmosphere.<sup>[5]</sup> Calculated values for temperatures at a location halfway between the electrode and the workpiece differed from the experimentally measured values<sup>[6]</sup> by 0 to 6.1 pct for currents of 150 A and 0 to 3.8 pct for currents of 250 A.<sup>[5]</sup> For this investigation, the model is applied to GMAW of mild steel.

### A. Mathematical Formulation of the Arc

The outline of the computational domain for the welding arc is shown in Figure 2, and the variables used in the figure are defined in the List of Symbols and in Table I. The following paragraphs summarize the important assumptions, equations, boundary conditions, and source terms used in the arc model. A more detailed description can be found in an earlier publication.<sup>[5]</sup>

The following assumptions are made in the mathematical model.

- (1) The arc is axially symmetric, so the governing equations can be written in two-dimensional cylindrical coordinates.
- (2) The operation of the arc is independent of time.
- (3) The arc is in local thermal equilibrium (LTE) (*i.e.*, the electron and heavy-particle temperatures are very similar). Hsu *et al.*<sup>[7]</sup> and Hsu and Pfender<sup>[8]</sup> show that this assumption is accurate through most of a gas tungsten arc, except near the anode and the cathode surfaces and in the fringes.
- (4) The gas flow is laminar. This can be justified in a similar way used by McKelliget and Szekely for a gas tungsten arc welding (GTAW) system on the basis of laminar-turbulent transition of a free jet.<sup>[9]</sup>

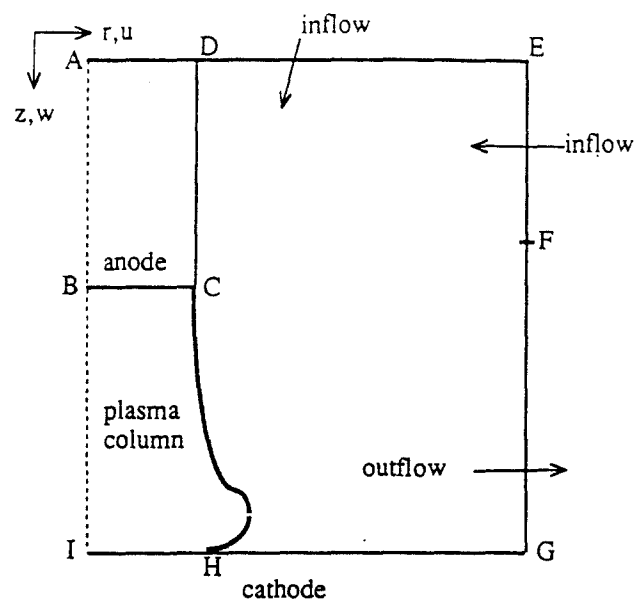


Fig. 2—Outline of the region of integration for the welding arc.

- (5) The plasma is optically thin so that radiation may be accounted for using an optical thin radiation loss per unit volume.
- (6) The consumable electrode is cylindrical and the tip of the electrode and the workpiece surfaces are flat.
- (7) The influence of metal droplets is neglected.
- (8) The consumable electrode is in a quasi-steady state.

#### 1. Transport equations for the arc

According to the preceding assumptions, the governing transport equations for the arc may be expressed in cylindrical coordinates as

Conservation of mass

$$\frac{1}{r} \frac{\partial(\rho r u)}{\partial r} + \frac{\partial(\rho w)}{\partial z} = 0 \quad [1]$$

where  $\rho$  is the mass density,  $r$  is the radial distance,  $z$  is the axial distance, and  $u$  and  $w$  are the radial and axial velocity components, respectively.

Conservation of radial momentum

$$\frac{1}{r} \frac{\partial(\rho r u^2)}{\partial r} + \frac{\partial(\rho u w)}{\partial z} = -\frac{\partial P}{\partial r} + \left[ \frac{2}{r} \frac{\partial}{\partial r} \left( \mu r \frac{\partial u}{\partial r} \right) - \mu \frac{2u}{r^2} + \frac{\partial}{\partial z} \left( \mu \left( \frac{\partial u}{\partial z} + \frac{\partial w}{\partial r} \right) \right) \right] - J_z B_\theta \quad [2]$$

where  $P$ ,  $\mu$ ,  $J_z$ , and  $B_\theta$  are the pressure, viscosity, axial current density, and self-induced azimuthal magnetic field, respectively.

Conservation of axial momentum

$$\frac{1}{r} \frac{\partial(\rho r u w)}{\partial r} + \frac{\partial(\rho w^2)}{\partial z} = -\frac{\partial P}{\partial z} + \left[ \frac{1}{r} \frac{\partial}{\partial r} \left( \mu r \left( \frac{\partial u}{\partial z} + \frac{\partial w}{\partial r} \right) \right) + 2 \frac{\partial}{\partial z} \left( \mu \left( \frac{\partial w}{\partial z} \right) \right) \right] + J_r B_\theta \quad [3]$$

where  $J_r$  is the radial current density.

Table I. Boundary Conditions for the Arc

Figure 2	$u$	$w$	$h$	$\Phi$
BC, CD, AD	0	0	$h_a$	0 (AD)
DE	0	$\frac{\partial \rho w}{\partial z} = 0$	$h_i$	$\frac{\partial \Phi}{\partial z} = 0$
EG	$\frac{\partial \rho u}{\partial r} = 0$	$\frac{\partial w}{\partial r} = 0$	$h_i$ (inflow) $\frac{\partial h}{\partial r} = 0$ (outflow)	$\frac{\partial \Phi}{\partial r} = 0$
IH	0	0	$h_{c,i}$	given by Eqs. [7] and [9]
HG	0	0	$h_{c,o}$	0

Conservation of thermal energy

$$\frac{1}{r} \frac{\partial(\rho r u h)}{\partial r} + \frac{\partial(\rho w h)}{\partial z} = \frac{1}{r} \frac{\partial}{\partial r} \left( k r \frac{\partial h}{\partial r} \right) + \frac{\partial}{\partial z} \left( k \frac{\partial h}{\partial z} \right) + \frac{J_r^2 + J_z^2}{\sigma_e} - S_R + \frac{5 k_b}{2 e} \left( \frac{J_r}{C_p} \frac{\partial h}{\partial r} + \frac{J_z}{C_p} \frac{\partial h}{\partial z} \right) \quad [4]$$

where  $h$  is the enthalpy,  $k$  is the thermal conductivity,  $C_p$  is the specific heat at constant pressure,  $\sigma_e$  is the electrical conductivity,  $S_R$  is the radiation loss term,  $k_b$  is the Boltzmann constant, and  $e$  is the elementary charge.

Conservation of charge continuity

$$\frac{1}{r} \frac{\partial}{\partial r} \left( \sigma_e r \frac{\partial \Phi}{\partial r} \right) + \frac{\partial}{\partial z} \left( \sigma_e \frac{\partial \Phi}{\partial z} \right) = 0 \quad [5]$$

where  $\Phi$  is the electrical potential.

The momentum equations consist of, from left to right, the two convective terms, the pressure gradient term, the diffusive term, and the electromagnetic body force term. The following energy equation consists of, from left to right, the two convective terms, the two diffusive terms, the Joule heating term, the radiation loss term, and the transport of enthalpy due to electron drift (Thompson effect). Finally, the charge continuity equation consists of two diffusive terms.

The current density,  $J$ , can be obtained from

$$J_r = -\sigma_e \frac{\partial \Phi}{\partial r} \quad [6]$$

$$J_z = -\sigma_e \frac{\partial \Phi}{\partial z} \quad [7]$$

while the self-induced azimuthal magnetic field,  $B_\theta$ , is derived from Ampere's law as

$$B_\theta = \frac{\mu_0}{r} \int_0^r J_z r dr \quad [8]$$

where  $\mu_0$  is the magnetic permeability of free space. The integration constant is assumed zero for  $B_\theta \rightarrow 0$  as  $r \rightarrow 0$ , since the integrand approaches zero as  $r \rightarrow 0$ .

2. Boundary conditions for the arc

A complete listing of the boundary conditions for the arc is presented in Table I, and the variables used in the table are defined in the List of Symbols.

Anode region (BC, CD, and AD)

A no-slip boundary condition is imposed for the momentum boundary conditions. The enthalpy boundary condition  $h_a$  is assumed to be the enthalpy corresponding to the melting temperature of pure iron, 1810 K. From a practical point of view, it is clear that the temperature in the anode varies, but this variation will not affect the studied arc characteristics. Initial sensitivity calculations, using anode temperature values ranging between 1000 to 1810 K, showed that the calculated maximum velocities and temperatures within a 225 A arc differed by less than 0.5 pct. The only equation solved for within the electrode region is the equation for the conservation of charge continuity. Here, the region AD is taken to be isopotential ( $\Phi = 0$ ). This is based on the assumption that the conductivity in the metal is much higher than in the plasma and that the variation of the electric potential in the metal is much less than in the arc.

Anode region, inflow (DE)

At the inflow region, the momentum boundary conditions are straight forward. The expression  $\partial(\rho w)/\partial z$  is the gradient of mass flow and is assumed to be zero. This is analogous to the expression  $\partial w/\partial z$ , except that the density term is included in the former expression to ensure mass conservation, since the density of gas is temperature dependent. The inlet gas enthalpy  $h_i$  is assumed to be the enthalpy corresponding to a temperature of 300 K. Initial sensitivity analyses of the temperature of the inlet gas within a range of 300 to 1000 K show that the arc behavior is not significantly affected. This has also been concluded by Hsu *et al.*<sup>[7]</sup>

Cathode region (GHI)

The no-slip conditions are used for the momentum equations at the solid boundaries. The cathode surface temperature is assumed to be the melting temperature of pure iron, 1810 K, within the cathode spot region (weld pool region). The cathode surface temperature outside the cathode spot region is arbitrarily assumed to be 1000 K. This value is based on results from a sensitivity calculation, which showed that the calculated maximum velocity and temperature values varied by less than 0.1 pct for temperature values of 700 to 1810 K. Based on these temperatures, the boundary conditions for the enthalpy within (IH),  $h_{c,i}$ , and outside (HG),  $h_{c,o}$ , the

cathode spot region are taken at temperature values of 1810 and 1000 K, respectively. The radius of the cathode spot,  $R_c$ , is defined as an average value representing the movement of the cathode spot. Theoretical calculations of the weld pool profiles showed that the weld pool radius is 3.2 to 3.5 mm for welding currents of 150 A to 220 A for an argon shielding gas.<sup>[10,11]</sup> Based on these values of the weld pool radius, a sensitivity calculation was done to study the effect of the cathode spot radius on the calculated arc characteristics. It was shown that the calculated maximum velocity varies less than 1.7 pct and the maximum temperature varies less than 0.1 pct for a 2.7 to 4.5 mm range of the cathode spot radius. Therefore,  $R_c$  was chosen as 2.7 mm in this investigation for the argon arc. For calculation of the helium arc, a cathode spot radius of 1 mm was used. This value represents the maximum value for which the numerical calculations in the current range 150 to 400 A converge. For larger values of the cathode spot radius, the arc voltage is not high enough to sustain the arc, which is seen from the failure to obtain a converged solution. Essentially, if the cathode spot power density is not sufficiently large, the temperature to sustain the plasma will not be produced and the arc will extinguish.

It is assumed that a single value of the current density is valid within the cathode spot (weld pool) region and that the current density is zero outside the cathode spot region. This assumption is based on the strong dependence of the current density on surface temperature; the temperatures in the weld pool region are substantially higher than in the rest of the workpiece. Therefore the current density conditions at the cathode are given by

$$J_c = \frac{I}{\pi R_c^2} \quad r \leq R_c \quad [9]$$

$$J_c = 0 \quad r > R_c \quad [10]$$

where  $J_c$  is the cathode current density and  $I$  is the welding current.

The electric potential boundary conditions at the cathode are derived using Eq. [7]. The value of the axial current density in Eq. [7] is taken as the cathode current density given by Eqs. [9] and [10].

#### Arc column (BI)

At the axis of symmetry, the following accepted boundary conditions are used: zero radial velocity at the axis and zero gradients of all other variable conditions normal to the axis.

#### Arc, inflow, and outflow (EG)

Since it is not clear where outflow and inflow will occur, zero radial mass flow gradient,  $(\partial(\rho u)/\partial r)$ , and electric potential gradients are specified at the boundary. The boundary condition for enthalpy representing mass flowing into the system is taken as  $h_i$ , which corresponds to a temperature value of 300 K. Although this value is arbitrary, initial calculations have shown that the arc behavior is not affected significantly by the choice of the enthalpy value. In fact, Hsu *et al.*<sup>[7]</sup> found that the computed argon arc behavior does not change significantly whether enthalpies corresponding to temperature values of 1000 or 2000 K are used. This is because the specific heat variation of argon outside the arc column is very

small (520 J/kg-K at 1000 to 6000 K compared to 9310 J/kg-K at 15,000 K) and does not represent a large change to the energy equation. Finally, for outflow, the expression  $\partial h/\partial r$  is assumed to be zero.

### 3. Source terms used at the cathode and the anode regions

#### Cathode

At the cathode boundary layer a nonthermal equilibrium (non-LTE) condition exists. This non-LTE condition is caused by a difference in temperature between electrons and heavy particles.<sup>[12]</sup> For thermionic cathodes found in GTAW, a positive source term is used to approximate the energy used in the cathode boundary layer to ionize the plasma (thereby causing a drop in the electric potential). This term is expressed as<sup>[7]</sup>

$$Q_c = |J_c| V_c \quad [11]$$

where  $V_c$  is the cathode fall voltage. However, in GMAW of iron the cathode is nonthermionic<sup>[13]</sup> and the cathode region is under high pressure due to the impinging plasma jet. The physics of the cathode-fall region and the thermal balance at a nonthermionic cathode are not very well understood.<sup>[14]</sup> Therefore, we have chosen to use a similar treatment of the energy source term at the cathode boundary as is used in GTAW. This will be an approximation, but initial sensitivity calculations showed that it will not affect the conditions in the arc column or in the anode region, where the highest temperatures exist. The following expression is used for the cathode fall voltage:<sup>[7]</sup>

$$V_c = \frac{5 k_b T_{c,e}}{2 e} \quad [12]$$

where  $T_{c,e}$  is the decrease in electron temperature at the cathode given as

$$T_{c,e} = T_{c,g} - T_{cat} \quad [13]$$

with  $T_{cat}$  being the temperature of the cathode, and  $T_{c,g}$  the temperature in the gas at a distance 0.1 mm from the cathode. This distance is the maximum experimentally observed thickness of the cathode fall region.<sup>[15]</sup>

#### Anode

The energy lost by the arc in the area close to the anode is due to electrical and thermal energy. The electrical energy is mainly transferred to the plasma (by making atoms vibrate faster) through joule heating. The effect of joule heating is accounted for in the equation for conservation of thermal energy. The enthalpy of the electrons are accounted for in the form of the Thompson effect (transport of enthalpy due to electron drift). The thermal energy loss in the arc at the anode boundary is in general due to a combination of conduction, convection, radiation, and vaporization. In this investigation, the heat loss due to radiation and vaporization in the anode boundary is neglected. Therefore, the heat loss in the arc at the anode boundary is due to the Thompson effect and the combined effect of conduction and convection. This heat loss is represented by the following expression:

$$Q_a = \frac{5 k_h}{2 e} (J_r [T_{a,g} - T_{an}] + J_c [T_{a,g} - T_{an}]) + k_g \frac{T_{a,g} - T_{an}}{\delta} \quad [14]$$

where the two terms represent the Thompson effect and the effect due to conduction and convection, respectively. In Eq. [14],  $T_{an}$  is the temperature of the anode and  $T_{a,g}$  is the temperature in the gas at a distance 0.1 mm from the anode. This distance  $\delta$  is the maximum experimentally observed thickness of the anode fall region.<sup>[15]</sup> The symbol  $k_g$  represents the thermal conductivity taken at an average temperature of the gas,  $T_{av}$ , given by

$$T_{av} = \frac{T_{a,g} + T_{an}}{2} \quad [15]$$

This approach is, of course, an approximation, since the parameters in Eq. [6] are dependent on the size of the anode fall region. However, sensitivity analyses showed that in combination, the parameters are less dependent on  $\delta$ . As a specific example, if the distance  $\delta$  is taken as 0.05 mm, the axial temperatures in the arc core are changed by 1.5 to 2.3 pct at locations 2.5 to 1.0 mm from the anode.

As a practical matter in the numerical solution of the equations, the Thompson effect, conduction, and convection are added as source terms in the first cell bordering the anode. The Thompson effect is accounted for as a source term throughout the computational domain, but its formal inclusion in Eq. [14] serves to emphasize its importance also at the phase boundary.

#### IV. THERMOPHYSICAL GAS PROPERTIES

The thermophysical properties of density, specific heat, and enthalpy for argon were taken from tabulated data of Liu.<sup>[16]</sup> The properties of molecular viscosity, thermal conductivity, and electrical conductivity for argon were taken from tabulated data of Devoto.<sup>[17]</sup> The radiation loss term  $S_R$  in the equation for conservation of energy was taken from experimental data of Evans and Tankin.<sup>[18]</sup>

All the thermophysical properties for pure helium, except radiation, are taken from tabulated data of Lick and Emmons.<sup>[19,20]</sup> The thermal conductivity and electrical conductivity for the 90 pct helium-10 pct iron vapor mixture are from data of Dunn and Eagar.<sup>[21]</sup> In the calculations using the helium-iron vapor mixture, the influence of the metal vapor upon the specific heat, enthalpy, molecular viscosity, and density for helium is not considered. The radiation loss term  $S_R$  for helium in the equation for conservation of thermal energy is taken from experimental data for argon of Evans and Tankin.<sup>[18]</sup> Emmons<sup>[22]</sup> pointed out that the radiation for helium is of the order of 1 pct of the total heat transfer in the arc. However, in this study, the radiation loss term for argon is used in the helium calculations, due to a lack of sufficient data for helium.

Initial calculations using thermophysical properties for pure helium did not converge. The cause is believed to be found in the electrical conductivity for helium. The

data for these properties are plotted against corresponding temperatures, along with data for argon, in Figure 3. The electrical conductivity for pure helium is so small at temperatures up to 8000 to 9000 K that an arc cannot be sustained. This has also been indicated by Emmons.<sup>[23]</sup>

Experimentally, it is known that gases like helium with a high ionization potential result in a less stable arc.<sup>[24]</sup> However, we also know that it is definitely possible to weld mild steel using helium as shielding gas. A likely cause of this is found in studying the influence of iron vapor (from electrode and workpiece) on the thermophysical properties. The following explanation is limited to iron vapor's influence on thermal and electrical conductivity, since these are the only thermophysical properties for which data are available.

Dunn<sup>[25]</sup> showed that even small amounts of iron vapor increase the electrical conductivity of helium at low temperatures, as is illustrated in Figure 4. It is seen that a 1 and 10 pct contribution of iron vapor have roughly a similar effect on the electrical conductivity. The effect of up to 10 pct iron concentrations on the thermal conductivity of helium is smaller than for the electrical conductivity, as is discussed subsequently. Therefore, iron vapor concentrations of between 1 to 10 pct in a helium gas are likely to have a very similar effect on the arc parameters. The values at a 10 pct iron vapor composition have been chosen in this investigation to represent GMAW of mild steel in a helium shielded atmosphere, and for simplification, "helium" will refer to this 90 pct helium-0 pct iron vapor shielding gas for the remainder of this article (with the exception of the discussion of Figure 5).

The rapid increase of the electrical conductivity with temperature in Figure 3 is due to ionization, which causes more electrons to be released from more frequent and energetic collisions. These highly mobile electrons are responsible for the flow of current between the anode and the cathode. At higher temperatures, the rate of increase in electrical conductivity with an increasing temperature is slowed down. This is thought to occur in relation to the completion of the first ionization.<sup>[23]</sup>

This influence of metal vapor on the properties of helium shielding gas refutes the traditional explanation that

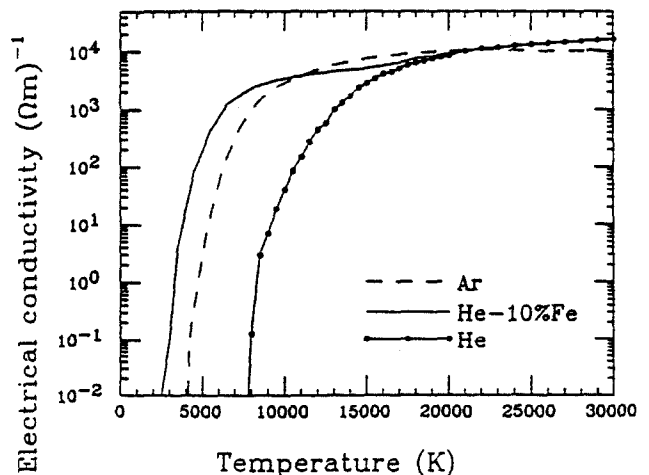


Fig. 3—Electrical conductivity as a function of temperature. Data for pure argon, pure helium, and a helium-10 pct iron vapor mixture.

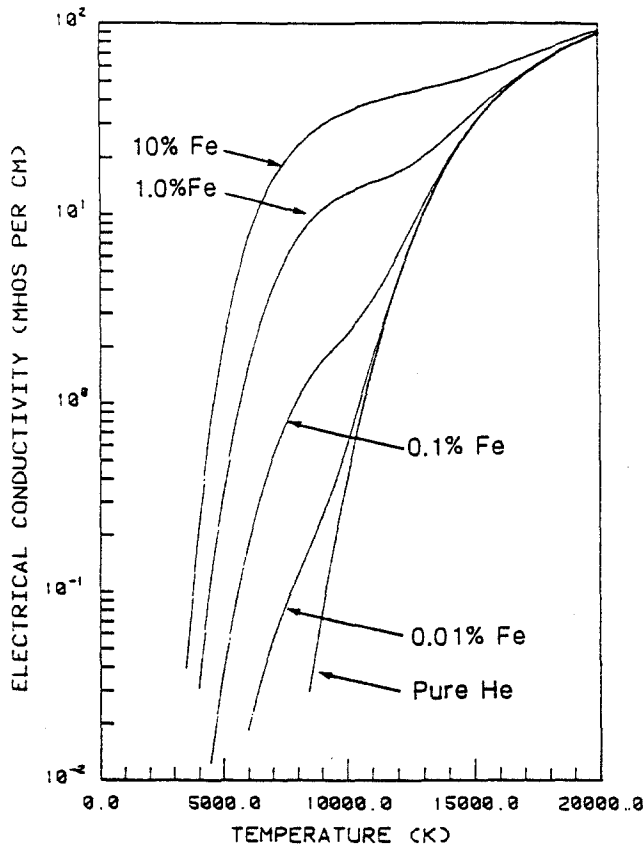


Fig. 4—Electrical conductivity as a function of temperature. Data for helium-iron vapor mixtures as reported by Dunn.<sup>1251</sup>

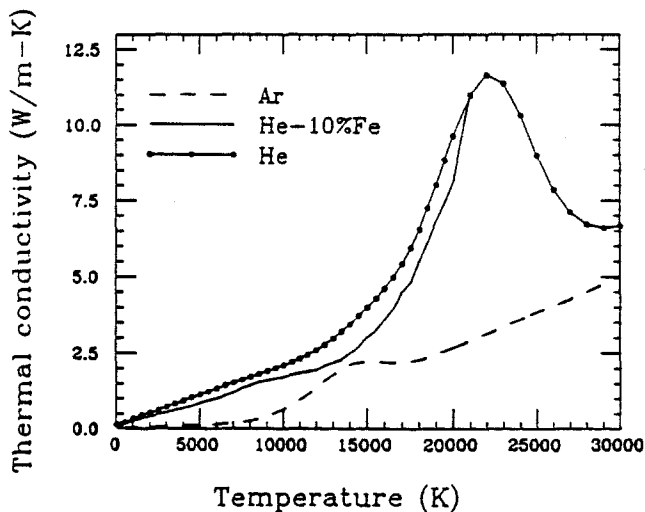


Fig. 5—Thermal conductivity data as a function of temperature for pure argon, pure helium, and a helium-10 pct iron vapor mixture.

it is the ionization potential of helium that increases the rate of heat transfer to the workpiece.<sup>1241</sup> The helium is not generally ionized in the welding arc.<sup>1251</sup> Eagar has proposed that it is the higher thermal conductivity of helium that increases the heat transfer to the workpiece.<sup>1261</sup>

The values of the thermal conductivity as a function of temperature are shown in Figure 5. Both the values representing pure helium and helium containing 10 pct

iron vapor are plotted along with the values for pure argon. As mentioned previously, the effect of a 10 pct iron addition to a helium gas has a minor effect on the thermal conductivity. The values for helium are higher than those for argon, especially at temperatures above 15,000 K. The values for helium increase up to a temperature of about 21,000 K, after which the thermal conductivity decreases. This occurs because the thermal conductivity is mainly determined by the diffusion of ionization energy; the change in thermal conductivity regarding temperature is small above about 21,000 K, because the gas is near to being completely ionized.<sup>1231</sup> A similar effect, but of smaller magnitude, is seen for argon at a temperature of approximately 14,500 K, when the first ionization is complete.<sup>1271</sup>

The density of argon is considerably higher than that of helium. At a temperature of 15,000 K, the density of argon is 6.4 times higher than for helium. The molecular viscosity for helium is larger than for argon at temperatures above about 9000 K and roughly the same at the lower temperatures.

The specific heat of helium is higher than that of argon. At its peak, around 22,000 K, the specific heat is 16.7 times higher than that of argon. The specific heat increases with temperature during ionization because a change in temperature requires that energy go into the ionization process.<sup>1231</sup> Therefore, the specific heat of helium decreases as the first ionization is nearly complete. The specific heat for argon has two peaks, one at about 14,500 K and the other at about 25,000 K, corresponding to the first and second ionization.

## V. NUMERICAL ANALYSIS AND RESULTS

### A. Solution Technique

The solution of the governing equations, boundary conditions, and source terms was obtained using a modified version of the software code 2/E/FIX, a two-dimensional, steady-state, fluid flow and heat transfer code based on a finite volume scheme.<sup>1281</sup> During a calculation, the finite difference equations were solved by iteration until they were satisfied within 99 pct. Satisfaction within 1.9 pct was also met for all current balance calculations. Since the nonlinear equations are highly temperature dependent, the relaxation parameters were continuously increased from values of 0.1 in the earlier iterations to values of 0.4 at later iterations. A typical calculation used a  $46 \times 34$  nonuniform mesh and required 40 to 80 minutes of CPU time on a Sun Sparcstation 10. In all calculations, the electrode diameter and arc length were kept at constant values of 1.14 and 4.75 mm, respectively. The studied current range was from 150 A to 400 A.

### B. Arc Parameters

Contour and vector plots for argon and helium-based shielding gases are presented at two different welding currents, 200 and 350 A. The absolute values of the electrical potential contours for helium are higher ( $\Phi_{\max} = 20.0$  V) than for argon ( $\Phi_{\max} = 11.1$  V) at a

200 A welding current. This is caused by the higher ionization potential (24.580 V for helium compared to 15.755 V for argon) that is required to strike and maintain an arc between the anode and the cathode. The voltage gradients are higher at the anode than in the arc column for both gases, and for helium this is also true at the cathode.

The high voltage gradients increase the current density since the latter is proportional to the gradient in electrical potential, as is shown in Eqs. 6 and 7. The absolute values of the radial  $F_r$  and axial  $F_z$  Lorentz forces in turn are proportional to the current density, which is seen from the following equations:

$$F_r = -J_z B_\theta \quad [16]$$

$$F_z = J_r B_\theta \quad [17]$$

Therefore, as expected, the plotted values of these electromagnetic body forces are also high near the anode for both gases and high near the cathode for helium, as shown in Figures 6(a) and (b). The Lorentz forces, in turn, affect the flow of mass in the arc because these forces are source terms in the momentum equations.<sup>[5]</sup>

The mass-flow vector plots for argon and helium are illustrated in Figures 7(a) and (b). In the argon arc, gas is entrained along the side of the electrode due to the Lorentz forces and accelerated from the electrode towards the workpiece, where it impinges and is directed towards the fringes of the system. In the helium arc, the gas is also entrained along the side of the electrode and accelerated towards the workpiece. However, this helium mass flow is counteracted by an opposite mass flow caused by the Lorentz forces at the cathode.

The mass flow patterns also affect the temperature distribution in the welding arc (Figures 8(a) and (b)). The fluid flow conditions in the argon arc cause hot gas to be transported from the electrode to the workpiece, and thereafter to the area parallel to the workpiece. This is indicated by the bell shape of the temperature contours in Figure 8(a). In the helium arc, the strong cathode force brings in cold gas from the fringes of the system to the

center of the arc, which can be seen by the shape of the contours.

At a 350 A welding current, a similar arc behavior is found as for a 200 A current, but the Lorentz forces at the anode increase more than at the cathode. Therefore, the mass flow in the helium arc (caused by the Lorentz forces close to the cathode) counteracts the mass flow originating from the anode to a smaller extent, as shown in Figures 9(a) and (b). The mass flow pattern for the argon arc is the same as at a 200 A current.

The change in mass flow in the helium arc at the higher current affects the temperature distribution, as well (Figure 10(b)). At this current, the temperature contours for the helium arc resemble the bell-shaped contours that are found in the argon system (Figure 10(a)).

### C. Metal Transfer

In the following section, both tapering of an electrode in an argon-shielded arc and repelled globular transfer of metal droplets in a helium-shielded arc are discussed, using predicted data of arc characteristics.

#### 1. Tapering of the electrode

It has been observed experimentally that the electrode becomes tapered at higher currents during GMAW of steel and aluminum using argon-based shielding gases.<sup>[29]</sup> Two recent in-depth investigations by Kim<sup>[29]</sup> and Kim *et al.*<sup>[30]</sup> suggest that the tapering is caused by condensation of electrons on the side of the electrode, which generates heat that in turn causes melting. The melted film has been reported to be transported to the tip of the electrode by either the combination of Lorentz, plasma drag, and gravitational forces<sup>[31]</sup> or by only gravitational and plasma drag forces.<sup>[29]</sup>

Using the developed arc model, it is possible to predict the percentage of electrons that will condense on the side of the electrode and the anode spot size, along with the arc forces acting at the electrode (for a given geometry of the electrode). The amount of electrons that condense on the anode, at equilibrium, corresponds to

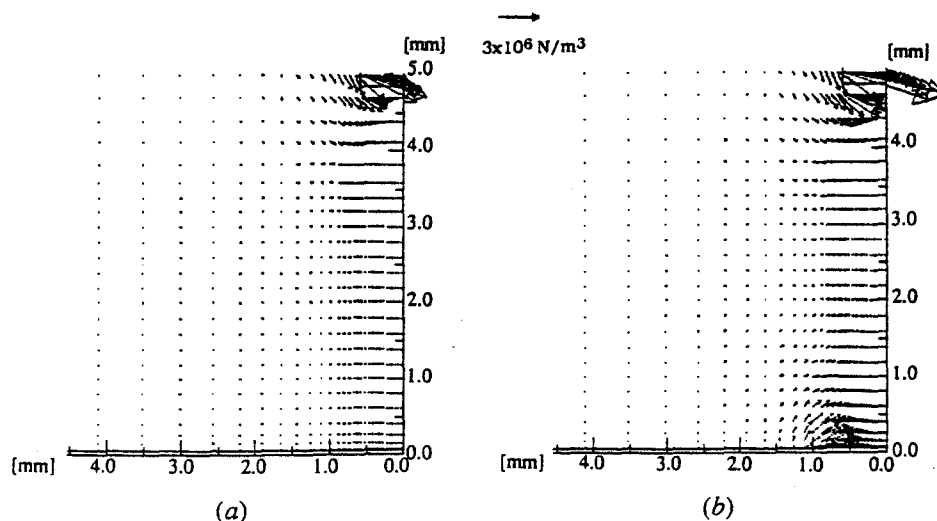


Fig. 6—Vector plots of the Lorentz force for (a) argon ( $F_{\max} = 1.1 \times 10^7 \text{ N/m}^2$ ) and (b) helium ( $F_{\max} = 1.1 \times 10^7 \text{ N/m}^2$ ) at a 200 A welding current.

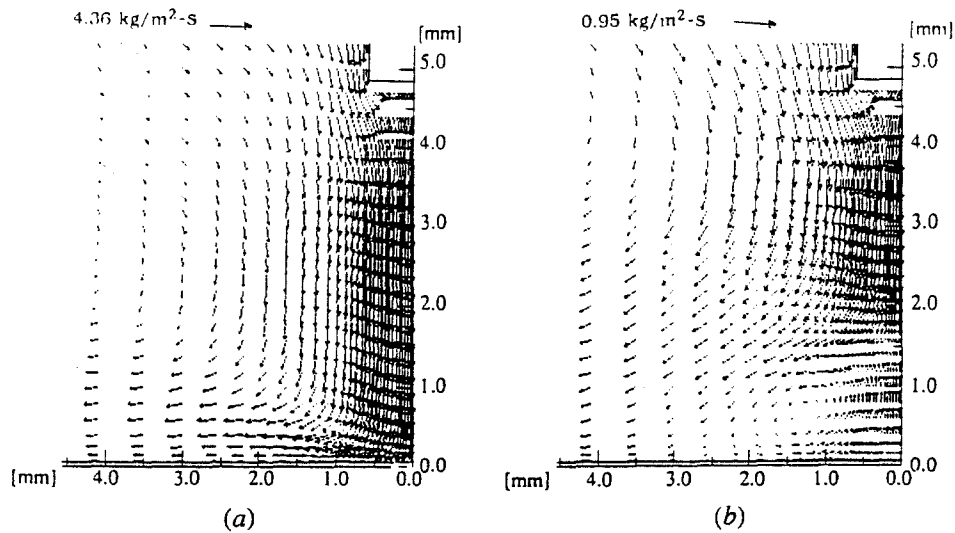


Fig. 7—Mass flow vector plots for (a) argon and (b) helium at a 200 A welding current. The maximum value in the GMAW system is given by the arrow.

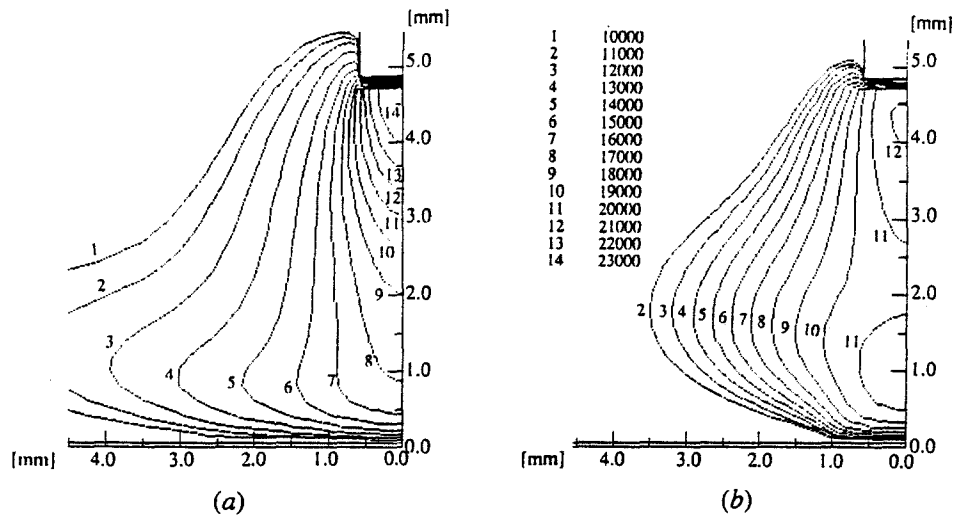


Fig. 8—Temperature contours for (a) argon ( $T_{max} = 23,970$  K) and (b) helium ( $T_{max} = 21,260$  K) at a 200 A welding current.

the amount of current that leaves the anode. Thus, the percentage of electrons that condense on the side of the electrode can be derived from the ratio of the calculated current that leaves the anode side and the total current leaving the anode. More specifically, the current at each calculation node is calculated as the product of the current density (from Eqs. [6] and [7]) and the area of the node at the gas-electrode boundary. (Note that Eq. [5], describing conservation of charge continuity, is solved for inside the electrode.) The anode spot size, on the side of the electrode, can be estimated as the distance from the anode tip to the node where the current is less than 0.1 pct of the total current leaving the anode side. In the following paragraphs, some results for GMAW of mild steel in argon and helium atmospheres are presented. The purpose is to discuss why tapering of the electrode is more likely to occur with argon than with helium shielding gases. All data, except for those in Figure 11, are taken at a welding current of 250 A.

Figure 11 illustrates the predicted percentage of electrons that condense on the side of the electrode versus current for a cylindrical geometry. In the studied current range of 150 to 400 A, the percentage of condensing electrons in the argon atmosphere is 25 to 49 pct larger than for the helium gas. The percentage of electrons that condenses on the side of the electrode, relative to the tip of the electrode, is proportional to the current flux leaving the electrode through its side. In plotting the calculated radial current density versus the axial distance from the tip of the electrode (Figure 12), it is clear that the radial current density is higher in the argon gas compared to the helium gas. From Figure 12, it is also seen that the current density becomes very small at a location 1.05 mm from the tip in the argon gas and 0.75 mm in the helium gas. This gives an indication of how far up on the electrode side the electrons condense, and therefore gives an indication of the extent to which the anode spot extends on the side of the electrode.



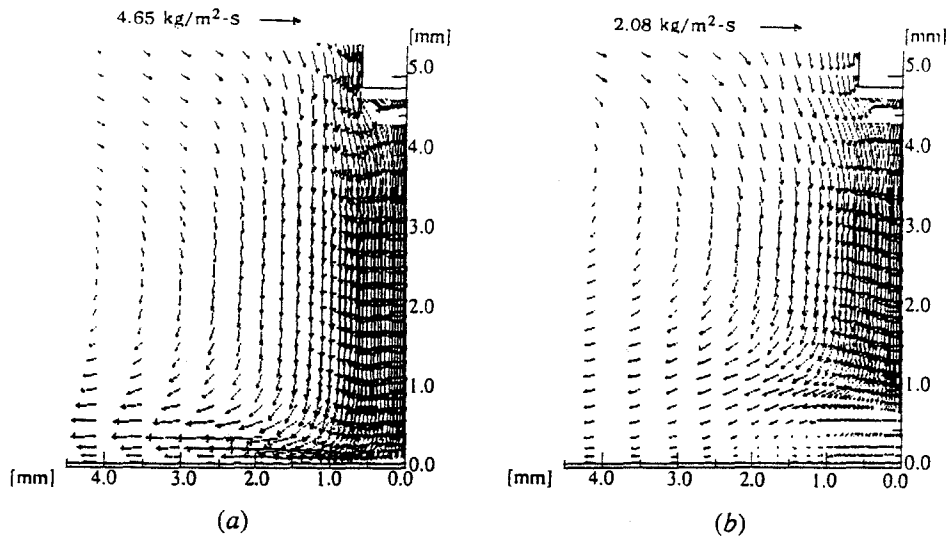


Fig. 9—Mass flow vector plots for (a) argon and (b) helium at a 350 A welding current. The maximum value in the GMAW system is given by the arrow.

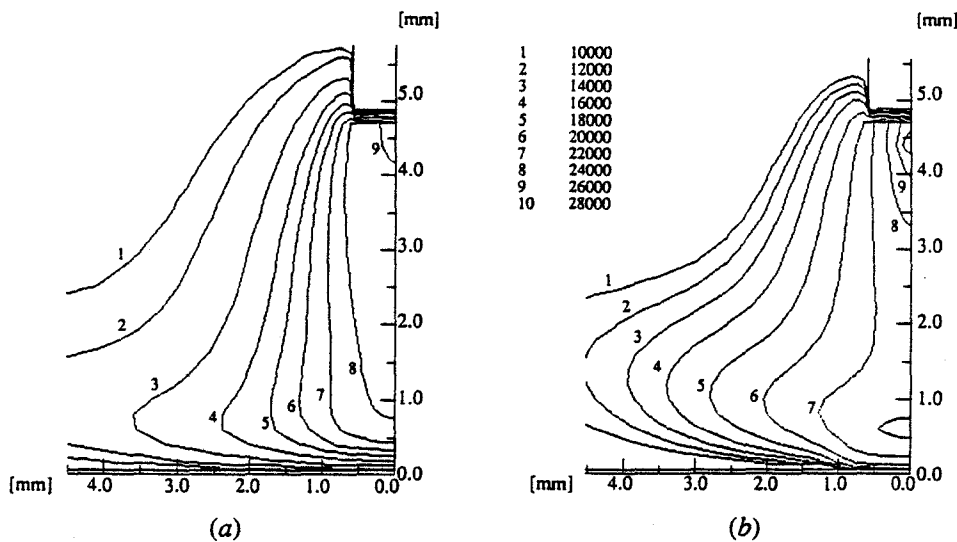


Fig. 10—Temperature contours for (a) argon ( $T_{\max} = 26,660$  K) and (b) helium ( $T_{\max} = 28,750$  K) at a 350 A welding current.

From Eqs. [6] and [7], it is seen that the current density is proportional to the electrical conductivity and the gradient in the electrical potential (electric field intensity). The plot of the numerically predicted electrical conductivity versus the axial distance from the electrode tip (Figure 13) shows that the values for argon are higher than the values for helium. The electrical conductivity varies with temperature, as shown in Figure 3. Therefore, the higher values of the electrical conductivity for argon, at the side of the electrode, are caused by the higher temperatures.

As mentioned previously, the current density is also proportional to the voltage gradient. Figure 14 shows that the calculated gradient in electrical potential is larger for helium than for argon. However, the effect of electrical conductivity on the current density is higher than the effect of the electric field intensity, since the current density values are lower for helium than for argon.

Previously, we also mentioned that between 25 and 49 pct more electrons condense on the side of the electrode in an argon shielding gas than a helium shielding gas. The higher degree of condensation in the argon gas generates more heat of condensation, which causes a higher degree of melting than for the helium shielding gas. As mentioned previously, the higher degree of melting in combination with the transport of liquid down to the electrode tip causes the tapering of the electrode. Up to now, it has not been clear which of the forces (Lorentz, plasma drag, or gravity) dominates the transport of liquid to the electrode tip. Gravity is probably the least important, since the thickness of the liquid film is small, about 0.1 mm.<sup>[29]</sup> Also, Kim<sup>[29]</sup> evaluated the relative contributions of the forces acting on a drop at the electrode tip using the static force balance theory. He found that the force due to gravity is the least important at all currents. The magnitude of the plasma drag forces per

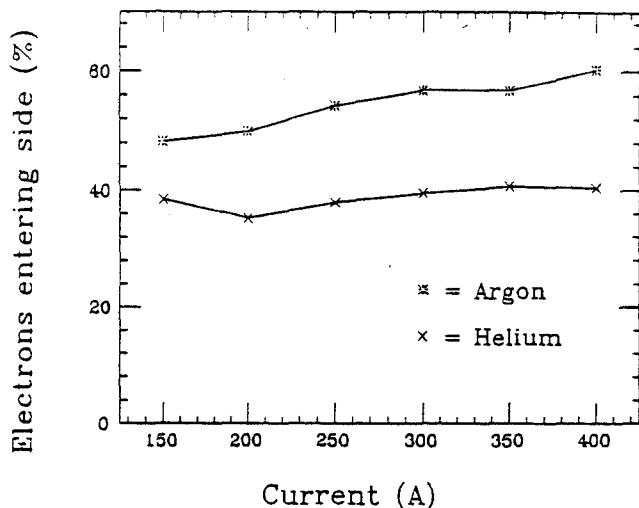


Fig. 11—The percentage of electrons that condense on the side of a cylindrical electrode as a function of the welding current.

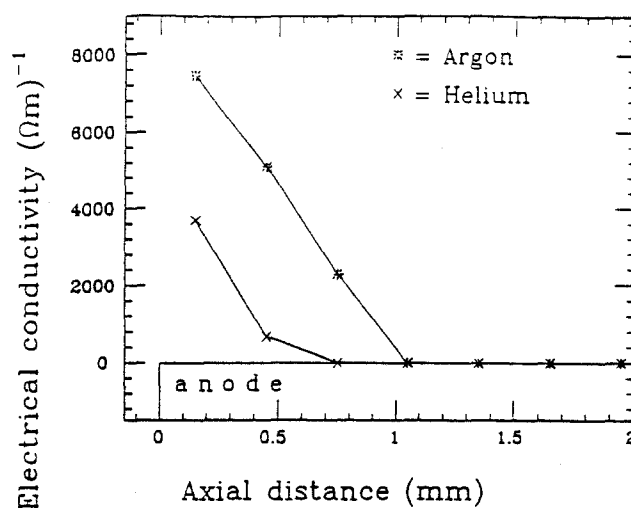


Fig. 13—The electrical conductivity as a function of the axial distance from the tip of the electrode. The welding current is 250 A. The data are taken at a radial location 0.025 mm from the side of the electrode.

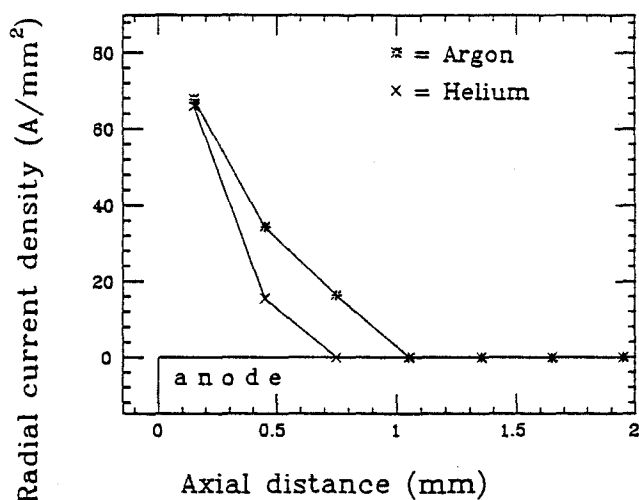


Fig. 12—The radial current density as a function of the axial distance from the tip of the electrode. The welding current is 250 A. The data are taken at a radial location 0.025 mm from the side of the electrode.

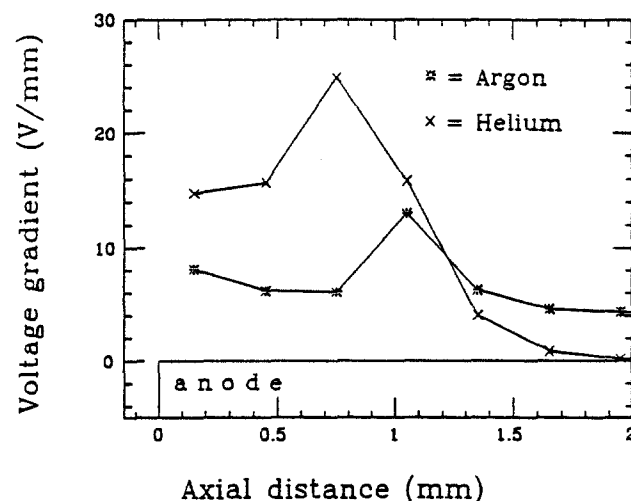


Fig. 14—The electric field intensity in the radial direction as a function of the axial distance from the tip of the electrode. The welding current is 250 A. The data are taken at a radial location 0.025 mm from the side of the electrode.

unit area and Lorentz forces per unit volume at a 250 A welding current are presented in the following paragraphs. The data are taken at a radial location 0.025 mm from the side of the electrode; the radial location is 0.625 mm from the axis of symmetry (the electrode radius is 0.6 mm).

The calculated axial plasma drag force per unit area (axial momentum flux) is shown as a function of axial distance for the argon and helium shielding gases in Figure 15. The axial momentum flux is very small along the side of the anode and at the cathode for both shielding gases. The values for the argon plasma are higher than the ones for the helium plasma. The maximum value of the axial momentum flux in the argon arc is 1075 N/m<sup>2</sup>, while the maximum value for the helium arc is roughly half that value, 591 N/m<sup>2</sup>. The predicted axial Lorentz force per unit volume is plotted in Figure 16 as a function of the axial distance. A negative

value indicates that the force is directed from the anode towards the cathode. For both gases, there is a peak force that pinches the anode tip at 3 N/cm<sup>3</sup>. A small force is also directed away from the cathode in the helium arc.

These results show that the magnitude of the axial Lorentz forces per unit volume is strongest at the anode tip, while the magnitude of the axial plasma drag forces per unit area are strongest in the plasma region between the anode and the cathode. Therefore, it is concluded that the Lorentz forces at least strongly dominate, if are not solely responsible for, the transport of the melted liquid from the side to the tip of the electrode.

## 2. Repelled globular transfer mode

It is well known that the phenomenon of repelled globular transfer occurs in GMAW of steel using a helium shielding gas.<sup>[32,33]</sup> Similar to the argon arc, in the

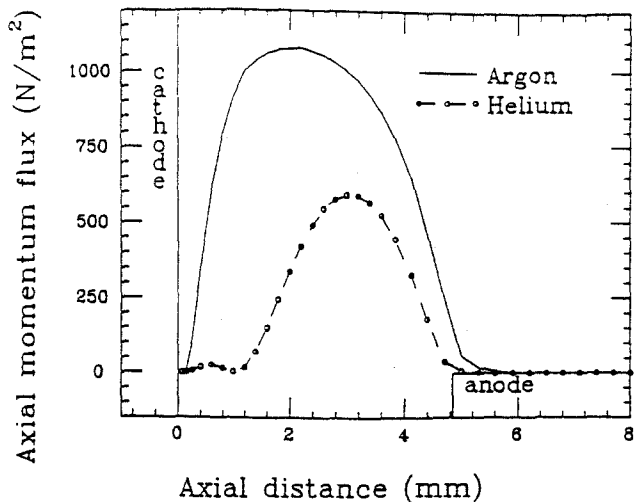


Fig. 15—The axial momentum flux as a function of the axial distance from the workpiece (cathode). The welding current is 250 A. The data are taken at a radial location 0.025 mm from the side of the electrode.

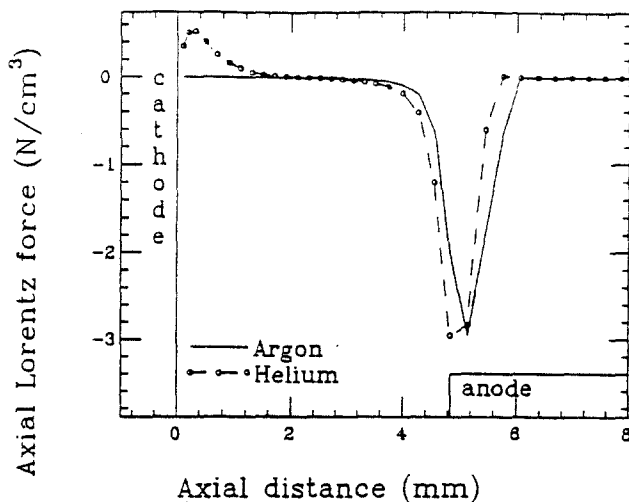


Fig. 16—The axial Lorentz force as a function of the axial distance from the workpiece (cathode). The welding current is 250 A. The data are taken at a radial location 0.025 mm from the side of the electrode.

helium arc, the melted film of the electrode forms droplets at the tip. Unlike the argon arc, however, the droplets formed in the helium arc are irregular in shape. This is caused by upward directed forces (repelling forces) acting on the droplets. The repelling forces furthermore cause the droplets to detach from the electrode in a randomly sideways direction. Some studies have mentioned the cathode force as the origin of the repelling force,<sup>[29,30]</sup> but no fundamental fluid flow and heat transfer study has confirmed this. From results presented in this study, it is concluded that a strong electromagnetic cathode force does exist (Figure 6(b)), supporting the cathode jet theory of Maecker.<sup>[34]</sup>

The mass flow caused by the cathode force counteracts the mass flow caused by the anode force, as is seen in Figure 7(b). Thus, the cathode force also plays a major role in the detachment of droplets from the molten electrode tip. Specifically, this upward force works against the anode forces that generate detachment in a downward motion. Furthermore, when the droplets are detached, they are not transferred to the workpiece area directly beneath the electrode tip but instead are dispersed randomly to the area surrounding the weld pool.

Figure 17 shows both the predicted maximum axial anode and cathode forces as a function of current. The absolute value of the anode force increases more rapidly with an increasing current than the absolute value of the cathode force does. Thus, the effect of the cathode force on the arc parameters becomes smaller with an increasing current (Figures 7(b) and 9(b) (mass flow) and Figures 8(b) and 10(b) (temperature)). Therefore, the tendency for repelled globular transfer will also decrease with an increasing current, which has also been observed experimentally.<sup>[29]</sup>

## VI. CONCLUSIONS

In this article we presented a mathematical formulation and computed results describing the behavior of the arc and the mechanism of metal transfer in the presence

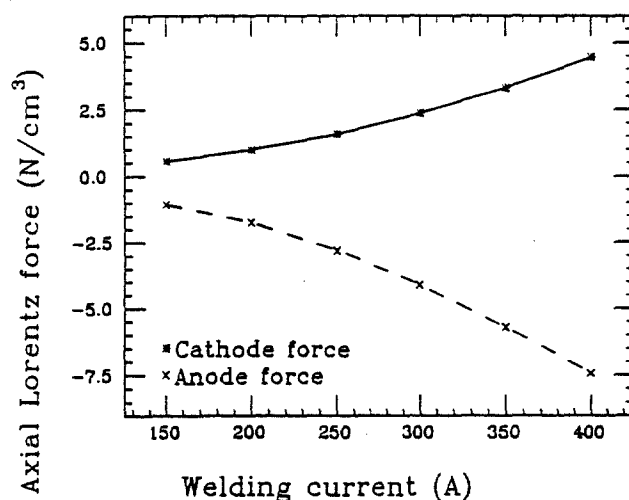


Fig. 17—The maximum axial anode and cathode Lorentz forces as a function of welding current for helium.

of an argon and a helium atmosphere. A key feature of the present work was that the arc system was represented using first principles through the simultaneous solution of the electromagnetic, heat flow, and fluid flow equations which in turn provided a basis for assessing the role of the gaseous environment in the process.

By examining the behavior of pure argon and pure helium as the gaseous environments, we were able to represent two extreme cases; argon is readily ionized and has an average thermal conductivity, while helium has a very high ionization potential but is an excellent conductor of thermal energy.

The general and perhaps most important finding was that the arcs behaved very differently for argon and helium atmospheres, which clearly confirms the widely held view that the shielding gas employed may have a pronounced effect on the overall performance of the system. More specifically, the model can readily explain experimental observations that for identical energy input

levels, melting will occur more rapidly in the presence of helium than argon. The model can also explain why the electrode tapers more significantly in the case of argon than for helium. Finally, the model can also explain the phenomenon of repelled metal transfer, *i.e.*, the ejection of metal droplets from the weld pool when using helium arcs.

Upon examining these points in detail, a key factor in the difference in behavior is attributable to the different thermophysical properties of argon and helium. Helium is difficult to ionize; indeed, the only reason that one can weld in a helium atmosphere is the presence of metal vapors that provide the necessary electric conductivity for the arc system. Thus, the role of metal vapors is an essential one in helium arcs and is much less critical for argon.

The fundamentally based quantitative representation of the system also allowed us to explain the experimentally observed electrode tapering phenomenon. With argon arcs, the overall temperature is much higher in the vicinity of the anode side (consumable electrode) and hence electrons can condense on the vertical walls of the feed wire. As a result, tapering of the electrode will occur. This tapering phenomenon is determined by two factors: one is the actual melting and the other is the transfer of the molten film to the tip of the electrode. While a detailed quantitative analysis of this phenomenon has not been performed up to the present time, it is plausible to consider that electromagnetic forces will play an important role in driving the flow of the molten metal film to the tip of the electrode. In the case of helium arcs, the temperatures at the anode side are lower and electrons will not condense on the vertical walls of the feed wire to the same extent, hence tapering is less likely to occur.

The model can also explain another interesting phenomenon that has been observed when using helium arcs, namely, repelled metal transfer. Here metal droplets are seen to be rejected from the metal pool. Calculations of the current density and electromagnetic force field profiles for the helium system have shown that because the cathode spot is quite small, there is a marked divergence (or convergence) of the current in the vicinity of the weld pool surface. It follows that this will lead to a high concentration of forces (clearly seen in Figure 6(b)), which in turn are responsible for repelled transfer.

In conclusion, one can state that by representing the arc phenomena on a fundamental basis in GMAW systems, we have the opportunity for developing explanations for a whole range of observed phenomena from first principles. The present work represents a first step in this direction, addressing the role of the shielding gas, or more appropriately, the gaseous environment of the arc, which is seen to play a very important role in determining the current path and nature of the electromagnetic forces. There is ample scope for the extension of this work to address the specific issues of the mechanism of electrode melting and the way in which these phenomena may be controlled. This will be the subject of continuing research within our group.

#### ACKNOWLEDGMENTS

The authors wish to thank the Materials Reliability Division at the National Institute of Standards and

Technology (NIST) in Boulder, CO, for financial support of this study. One of the authors (PGJ) gives special thanks to his wife, Sherri Valencik, for proofreading and textual editing of the manuscript.

#### LIST OF SYMBOLS

$B_\theta$	self-induced azimuthal magnetic field (Wb/m <sup>2</sup> )
$C_p$	specific heat at constant pressure (J/kg K)
$e$	elementary charge (As)
$F_r$	radial Lorentz force (N/m <sup>3</sup> )
$F_z$	axial Lorentz force (N/m <sup>3</sup> )
$h$	plasma enthalpy (J/kg)
$h_a$	anode enthalpy (J/kg)
$h_{c,i}$	enthalpy within the cathode spot region (J/kg)
$h_{c,o}$	enthalpy outside the cathode spot region (J/kg)
$h_i$	enthalpy of gas flowing into the system (J/kg)
$I$	welding current (A)
$J$	current density (A/m <sup>2</sup> )
$J_c$	cathode current density (A/m <sup>2</sup> )
$J_r$	radial current density (A/m <sup>2</sup> )
$J_z$	axial current density (A/m <sup>2</sup> )
$k$	thermal conductivity (W/m K)
$k_b$	Boltzmann's constant (J/K)
$k_g$	thermal conductivity in the anode fall region (W/m K)
$P$	pressure (Pa)
$Q_a$	heat lost by the gas in the anode fall region (W/m <sup>2</sup> )
$Q_c$	heat gained by the gas in the cathode fall region (W/m <sup>2</sup> )
$r$	radial distance (m)
$R_c$	cathode spot (weld pool) radius (m)
$S_R$	radiation loss term (W/m <sup>3</sup> )
$T$	temperature (K)
$T_{a,g}$	temperature in the gas at a distance $d$ from the anode (K)
$T_{an}$	anode temperature (K)
$T_{av}$	average temperature of gas in the anode fall region (K)
$T_{c,e}$	decrease in electron temperature at the cathode (K)
$T_{c,g}$	temperature in the gas at a distance 0.1 mm from the cathode (K)
$T_{cat}$	cathode temperature (K)
$u$	radial velocity (m/s)
$V_c$	cathode fall voltage (V)
$w$	axial velocity (m/s)
$z$	axial distance (m)

#### Greek symbols

$\delta$	thickness of anode fall region (m)
$\mu$	molecular dynamic viscosity (Kg/ms)
$\mu_0$	magnetic permeability of free space (H/m)
$\rho$	density (kg/m <sup>3</sup> )
$\sigma_e$	electrical conductivity (1/Wm)
$\Phi$	electric potential (V)
$\Phi_{max}$	maximum value of the electric potential (V)

## REFERENCES

1. *Welding Handbook*, L.P. Kearns, ed., American Welding Society, Miami, FL, 1978, vol. II, pp. 131-37.
2. *The Physics of Welding*, J.F. Lancaster, ed., Pergamon Press, Oxford, United Kingdom, 1986, p. 15.
3. V.R. Dillenbeck and L. Castagno: *3rd Int. Conf. on Welding and Performance of Pipelines*, The Welding Institute, London, 1986, pp. 221-32.
4. J. Norrish: *Advanced Welding Processes*, Institute of Physics Publishing, Bristol, United Kingdom, 1992, p. 83.
5. P.G. Jönsson, R.C. Westhoff, and J. Szekely: *J. Appl. Phys.*, 1993, vol. 74, pp. 5997-6006.
6. E.A. Smårs and K. Acinger: Report No. 212-162-68, International Institute of Welding, Abington, United Kingdom, 1968.
7. K.C. Hsu, K. Etemadi, and E. Pfender: *J. Appl. Phys.*, 1983, vol. 54, pp. 1293-301.
8. K.C. Hsu and E. Pfender: *J. Appl. Phys.*, 1983, vol. 54, pp. 4359-66.
9. J. McKelliget and J. Szekely: *Metall. Trans. A*, 1986, vol. 17A, pp. 1139-48.
10. T. Zacharia, A.H. Eraslan, and D.K. Aidun: *Weld. J.*, 1988, vol. 68, pp. 18s-27s.
11. K.C. Tsao and C.S. Wu: *Weld. J.*, 1988, vol. 68, pp. 70s-75s.
12. K.C. Hsu and E. Pfender: *J. Appl. Phys.*, 1983, vol. 54, pp. 3818-24.
13. P.G. Jönsson: Ph.D. Thesis, Massachusetts Institute of Technology, Cambridge, MA, 1993.
14. *The Physics of Welding*, J.F. Lancaster, ed., Pergamon Press, Oxford, United Kingdom, 1986, pp. 120-227.
15. W. Finkelburg and S.M. Segal: *Phys. Rev.*, 1951, vol. 83, pp. 582-85.
16. C.F. Liu: Ph.D. Thesis, University of Minnesota, Minneapolis, MN, 1977.
17. R.S. Devoto: *Phys. Fluids*, 1973, vol. 16, pp. 616-23.
18. D.L. Evans and R.S. Tankin: *Phys. Fluids*, 1967, vol. 10, pp. 1137-44.
19. W.J. Lick and H.W. Emmons: *Thermodynamic Properties of Helium to 50000 K*, Harvard University Press, Cambridge, MA, 1962, pp. 35-37.
20. W.J. Lick and H.W. Emmons: *Transport Properties of Helium from 200 to 50000 K*, Harvard University Press, Cambridge, MA, 1962, pp. 87-89.
21. G.J. Dunn and T.W. Eagar: *Metall. Trans. A*, 1986, vol. 17A, pp. 1865-71.
22. H.W. Emmons: *Phys. Fluids*, 1967, vol. 10, pp. 1125-36.
23. H.W. Emmons: in *Modern Developments in Heat Transfer*, W. Ibele, ed., Academic Press, New York, NY, 1963, pp. 413-25.
24. *Welding Handbook*, C. Weisman, ed., American Welding Society, Miami, FL, 1976, vol. 1.
25. G.J. Dunn: M.A. and B.A. Thesis, Department of Materials Science and Engineering, Massachusetts Institute of Technology, Cambridge, MA, 1984.
26. T.W. Eagar: *Recent Trends in Welding Research*, S.A. David and J.M. Vitek, eds., ASM, Materials Park, OH, 1990, pp. 1-6.
27. P. Fauchais, M. Boulos, and E. Pfender: *Plasma Technology in Metallurgical Processing*, Iron and Steel Institute, Warrendale, PA, pp. 11-26.
28. W.M. Pun and D.B. Spalding: Report No. HTS/76/2, Imperial College, London, 1976.
29. Y.-S. Kim: Ph.D. Thesis, Department of Materials Science and Engineering, Massachusetts Institute of Technology, Cambridge, MA, 1989.
30. Y.-S. Kim, D.M. McEligot, and T.W. Eagar: *Weld. J.*, 1991, vol. 70, pp. 20s-31s.
31. C.J. Cooksey and D.R. Milner: *Physics of the Welding Arc*, The Institute of Welding, London, 1962, pp. 123-32.
32. T.B. Hazlett and G.M. Gordon: *Weld. J.*, 1957, vol. 36, pp. 382s-386s.
33. L.F. Defize: *Physics of the Welding Arc*, The Institute of Welding, London, 1962, pp. 112-14.
34. H. Maecker: *Zeitschrift für Physik*, 1955, vol. 141, pp. 198-216.